DOI 10.31489/2021Ph3/101-114
UDC 669.295:539.214

[1]V.M. Yurov[*], [2]A.T. Berdibekov, [3]N.A. Belgibekov, [1]K.M. Makhanov

[1]Karagandy University of the name of academician E.A. Buketov, Kazakhstan;
[2]MTO of the National University of Defense named after the First President of the Republic of Kazakhstan — Elbasy
[3]LLC «Research & Development Center» Kazakhstan Engineering»
*(*e-mail: exciton@list.ru)*

High entropic coatings FeCrNiTiZrAl and their properties

In our proposed empirical model, the anisotropy of the surface energy and the thickness of the surface layer of the high-entropy FeCrNiTiZrAl alloy are calculated. The thickness of the surface layer of this alloy is about 2 nm, which is an order of magnitude greater than the thickness of the surface layer of complex crystals, but is of the same order of magnitude as that of metallic glasses. The hardness and other properties of the high-entropy alloy are the same as for metallic glasses, but are 2-3 times higher than the hardness of stainless steels. The surface energy of the high-entropy FeCrNiTiZrAl alloy is about 2 J/m2, which corresponds to the surface energy of magnesium oxide and other crystals with a high melting point. However, unlike these crystals, the friction coefficients of a high-entropy alloy (~ 0.06) are much lower than that of ordinary steels (~ 0.8). We have theoretically shown that the friction coefficient is proportionally dependent on the surface energy and inversely proportional to the Gibbs energy, which significantly decreases for a high-entropy alloy, leading to low friction. The high hardness and low coefficient of friction of the high-entropy alloy facilitates the deposition of coatings from them on structural metal products, which contributes to their widespread use.

Keywords: high-entropy coatings, hardness, friction, wear resistance, nanostructure, microhardness.

Introduction

In high-entropy alloys, as a result of the effect of intense mixing, the entropy contribution increases, which stabilizes the formation of a solid solution with a simple structure [1-3]. Based on Boltzmann's hypothesis on the relationship between entropy and system complexity, the configurational change in entropy ΔS_{conf} during the formation of a solid solution of n elements with equiatomic content can be calculated using the following formula:

$$\Delta S_{conf} = -R \ln(1/n) = R \ln(n), \quad (1)$$

where R is the universal gas constant, n is the number of mixing elements.

At n = 5, ΔS_{conf} = 1.61R approaches the value of the melting entropy of most intermetallics (about 2R). However, it was later shown that a high entropy of mixing is not a necessary condition for the formation of a single-phase solid solution, but the very term for the name of such an alloy continues to remain in use [4-9]. There are foreign reviews and some dissertations on high-entropy alloys [10-12], but research in this direction is only gaining momentum. We also investigated some high-entropy alloys and coatings obtained by mechanical alloying and magnetron sputtering of targets [13-15].

In our proposed empirical model, not only the anisotropy is calculated, but also the thickness of the surface layer of the high-entropy alloy [16-18].

Objects and research methods

To prepare the FeCrNiTiZrAl target the corresponding equiatomic metal micropowders were used. Further, the obtained metal composition was loaded into a mill glass, which was made of tungsten carbide, and grinding balls with a diameter of 5-10 mm were also made of tungsten carbide. Having filled the glass of the mill with Galosha gasoline, the mill was connected to the rotation connector at a speed of 500 revolutions/minute for 5 hours. Then the metal composition was dried, pressed into a disc 100 mm in diameter and 5 mm thick, and placed in a thermal furnace in which the required vacuum was maintained. The process itself took 3 hours. The FeCrNiTiZrAl target was used in the deposition of coatings (Fig. 1).

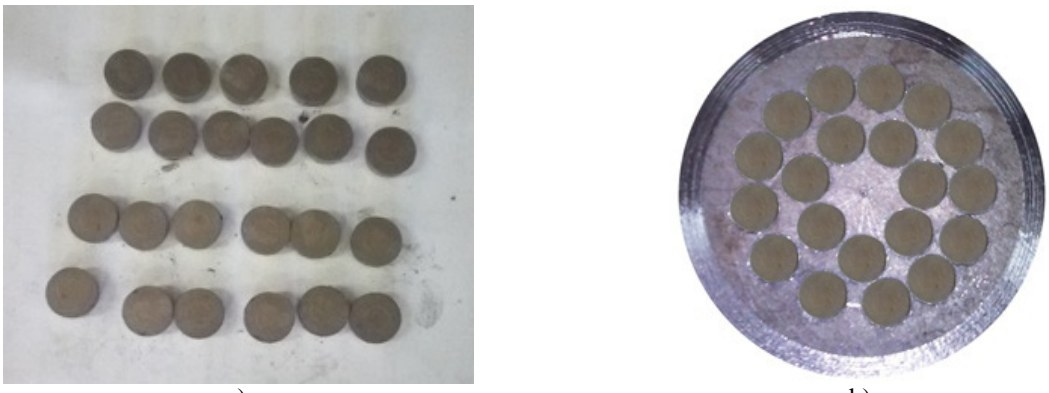

a) b)

Figure 1. Tablets from FeCrNiTiZrAl alloy (a), target with tablets from FeCrNiTiZrAl alloy (b)

Electron microscopic examination was carried out on a scanning electron microscope (SEM) MIRA 3 from TESCAN (Fig. 2).

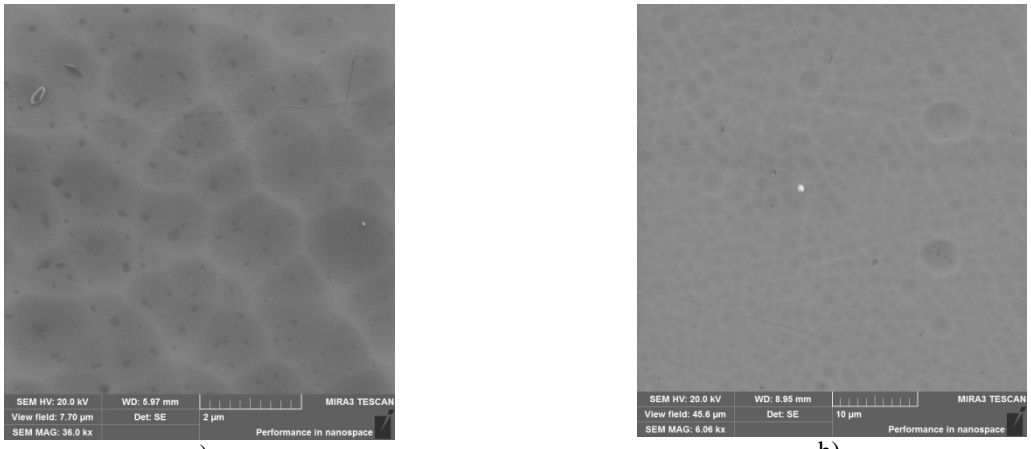

a) b)

Figure 2. SEM image of the FeCrNiTiZrAl coating in argon 2 µm (a) and 10 µm (b)

X-ray fluorescence electron spectroscopy (XPS) of FeCrNiTiZrAl coatings for argon is shown in Figure 3, and the chemical composition is presented in Table 1.

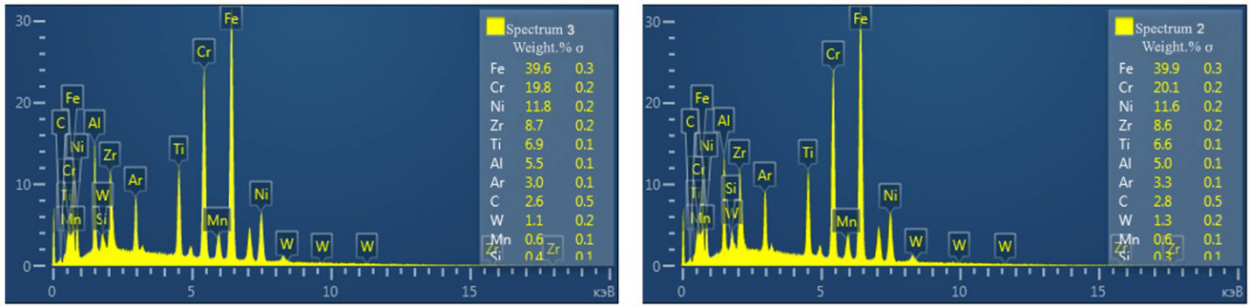

Figure 3. XPS of FeCrNiTiZrAl coatings at two points

Table 1

Chemical composition of the target (at.%)

Alloy	Fe	Cr	Ni	Ti	Zr	Al
FeCrNiTiZrAl	39,6	19,8	11,8	6,9	8,7	5,5

The chemical composition (Table 1) indicates that we have a high-entropy alloy (5-40 at.%). The obtained values of the mass concentration of the elements of the composite cathodes were used to calculate their stoichiometry in the analyzed compound. The values of mass concentration at. % of elements are taken from the experimental data (Fig. 3 and Table 1) — $Fe_{39.6}Cr_{19.8}Ni_{11.8}Ti_{6.9}Zr_{8.7}Al_{5.5}$.

Investigations of the morphology (Fig. 4) of the FeCrNiTiZrAl surface obtained by magnetron sputtering in vacuum were carried out on a JSPM-5400 atomic force microscope (AFM) manufactured by JEOL.

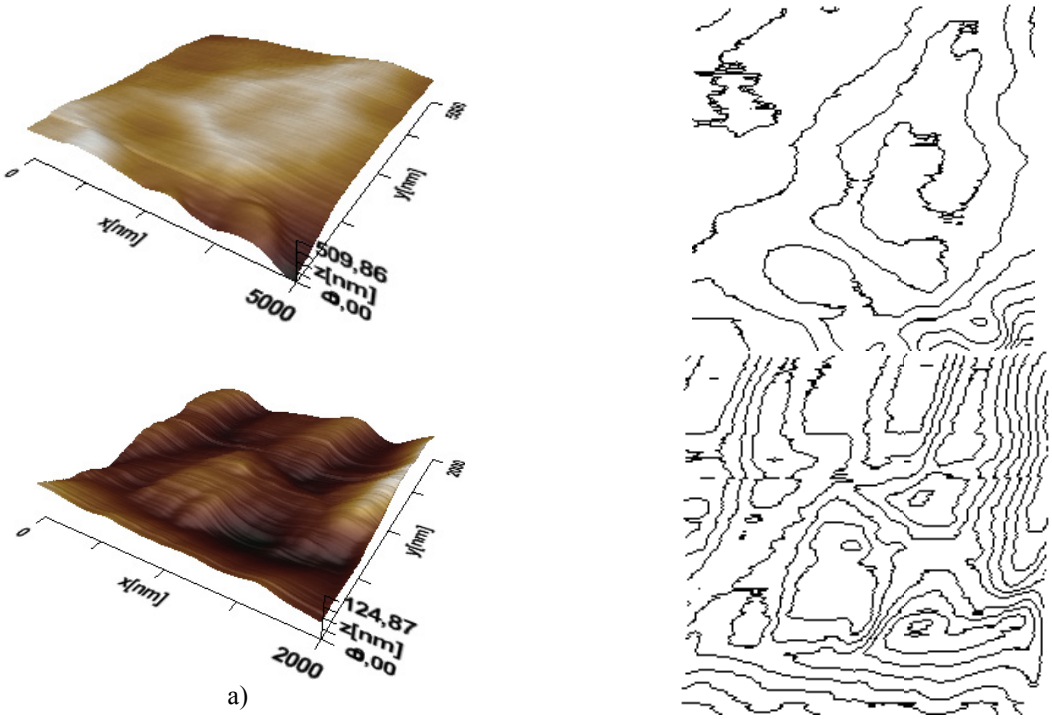

a) b)

Figure 4. AFM image of the FeCrNiTiZrAl surface (a) and its fractal structure (b) at two points

We used HVS-1000A microhardness tester (Fig. 5a). This instrument is designed using the latest advances in mechanics, optics, electronics and computer technology to test the hardness of metallic and non-metallic materials, especially small parts or thin hardened layers. The general scheme of the installation for determining the friction coefficients is shown in Figure 5b and includes: 1 — known clamping weight (15-25 mg), 2 — sample, 3 — sliding surface, 4 — measuring table, 5 — force transducer, 6 — electronics unit and drive.

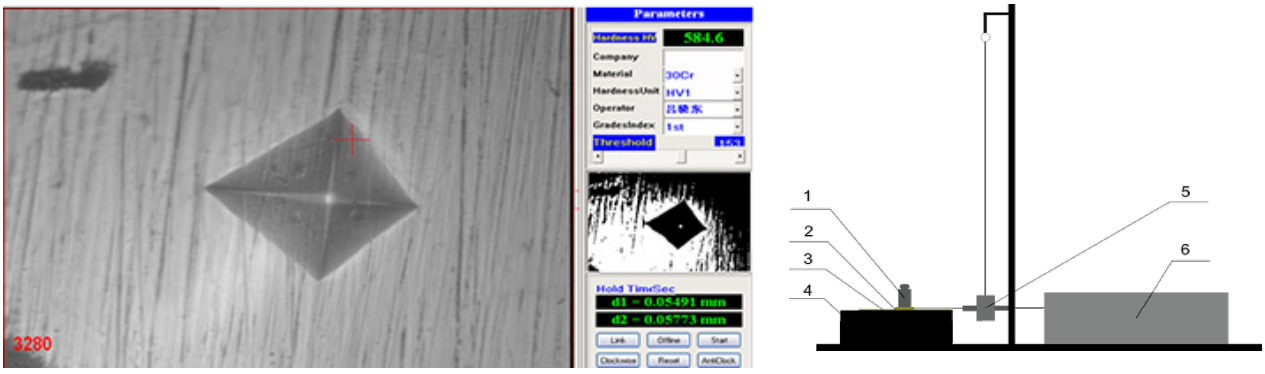

a) b)

Figure 5. Microhardness tester HVC-1000A (a) and installation diagram for determining the friction coefficients (b)

Calculations of the surface energy will be carried out according to the formula derived under the assumption that there are no first-order phase transitions in these substances up to their melting point [16]:

$$\sigma_{hkl} = \left(\frac{\rho l_{hkl}}{M}\right)\int_o^{T_m} c_p dT, \tag{2}$$

where ρ is the density of the crystalline substance, and M is its molecular weight, Tm is the melting point, cp is the molar heat capacity, l_{hkl} is the thickness of the first coordination sphere in the [hkl] direction, which for crystals with body-centered (bcc) and face-centered (fcc)) is given by the relations [19, 20]:

$$\begin{aligned} &\text{Im}3\text{m},\ Z = 2;\ l_{100} = a;\ l_{110} = a\sqrt{2};\ l_{111} = a/\sqrt{3}, \\ &\text{Fd}3\text{m},\ Z = 4;\ l_{100} = a;\ l_{110} - a/\sqrt{2};\ l_{111} = 2a/\sqrt{3}. \end{aligned} \tag{3}$$

The parameter R(I) is related to the surface energy σ. In [18] we showed that the following relation is fulfilled with an accuracy of 3%:

$$\sigma = 10^{-3}\cdot T_{\text{m}}, \tag{4}$$

where T_m is the melting point of the solid (K). The ratio is fulfilled for all metals and for other crystalline compounds. For $T = T_m$ from [18] we get:

$$\text{R(I)}_{\text{i}} = 0.24\cdot 10^{-9}\upsilon. \tag{5}$$

Equation (5) shows that the surface layer of thickness R(I) is determined by the molar (atomic) volume of the element υ = M/ρ, M is the molar mass (g/mol), ρ is the density (g/cm^3), which periodically changes in accordance with the table D.I. Mendeleev. For HEAs, the following ratios are valid:

$$\begin{aligned} T_m &= \sum_{i=1}^{n} c_i (T_m)_i, \\ M &= \sum_{i=1}^{n} c_i (M)_i, \\ \rho &= \sum_{i=1}^{n} c_i (\rho)_i, \end{aligned} \tag{6}$$

where $(T_m)_i$ is the melting point of each alloy element (K), $(M)_i$ is the molar mass of each alloy element (g/mol), ρ is the density of each alloy element (g/cm^3), ci is the concentration of each alloy element, n is the number of alloy elements. All these calculations are carried out using Table 1. Equation (4) can be rewritten as:

$$\sigma(\text{hkl}) = 10^{-3}\cdot T_{\text{m}}\cdot \text{l(hkl)}, \tag{7}$$

where l (hkl) for crystals with body-centered (bcc) and face-centered (fcc) cubic structures is given by relations (3) at a = 1.

Experimental results and their discussion

Let's make calculations according to (5), (6) and (7), taking reference data on T_m, M, ρ [21].

Table 2

Surface layer thickness and surface energy anisotropy FeCrNiTiZrAl

Alloy	(hkl)	Structure	T_m, K	R(I), nm	σ_{hkl} mJ/m^2
FeCrNiTiZrAl	100	Fd3m	1644	1,9	1644
	110			1,4	1174
	111			2,2	1934

Our proposed empirical model is schematically shown in Figure 6. It is an ideal atomically smooth single crystal without vacancies, dislocations and other defects.

The de Broglie layer $R_0 = \lambda dB = \hbar/p$ for metals ranges from 0.01 nm to 0.1 nm. Quantum dimensional effects begin in this layer. The main quantum-dimensional structures include structures with a two-dimensional electron gas — epitaxial films, MIS structures, heterostructures, etc.; structures with one-dimensional gas — quantum threads or wires; structures with zero-dimensional gas — quantum dots, boxes, crystallites [22].

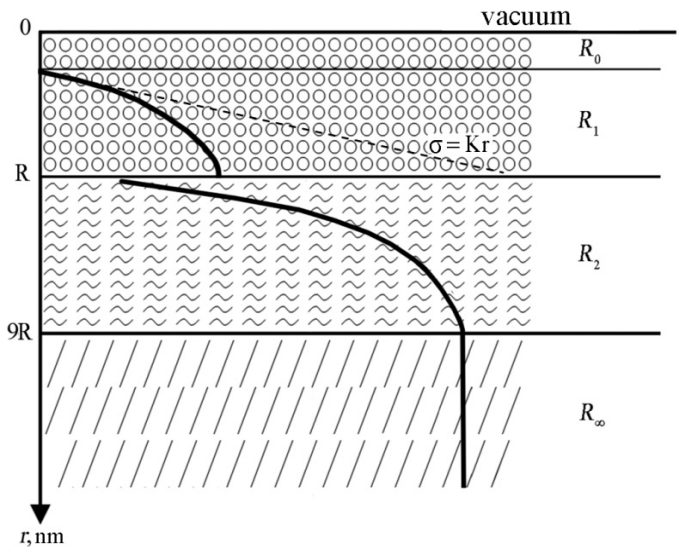

R_0 — de Broglie layer; R_1 — layer R(I); R_2 is the R(II) layer; R_∞ — solid sample layer

Figure 6. Schematic representation of the surface layer [18].

In the R(I) layer with pure metal atoms, there is a reconstruction and relaxation associated with the rearrangement of the surface [23]. For gold, the lattice constant is equal to a = 0.41 nm and the surface is rearranged at a distance $R(I)_{Au}$ = 1.2/0.41≈3 three atomic monolayers. The size effects in the R(I) layer are determined by the entire collective of atoms in the system (collective processes). Such «semiclassical» size effects are observed only in nanoparticles and nanostructures [24]. Experimentally, they can be observed in very pure single crystals, when the regime of grazing incidence of X-ray radiation is observed and in the case of an angle of incidence equal to or obviously smaller than the critical angle with total internal reflection [25]. In this case, the refractive wave decays exponentially at sizes on the order of a nanometer. For example, this dimension is 3.1 nm for silicon and 1.2 nm for gold. The result of this process is wave motion, which propagates along the surface and reflects the thickness of the surface layer [23].

The R(II) layer extends approximately to the size R(II) ≈ 9R = R_∞, where the bulk phase begins. Dimensional properties begin from this size. By nanomaterials it is customary to understand materials, the main structural elements of which do not exceed the nanotechnological boundary of ~ 100 nm, at least in one direction [25-27].

Table 2 shows that the structure of FeCrNiTiZrAl has a surface layer thickness of about 2 nm on average, which is 5-6 monolayers and is a nanostructure.

Considering the case when the alloy is formed from its constituent elements under isobaric conditions, the change ΔGmix of mixing from the initial element-by-element state to the state after fusion can be expressed as:

$$\Delta G_{mix} = \Delta H_{mix} - T\Delta S_{mix}. \quad (8)$$

An equilibrium state is a state with a minimum of free energy. Figure 7a (according to equation 1) shows an increase in the entropy of mixing with an increase in the number of elements for equimolar alloys. It is seen that the entropy of mixing for the phases of the solid solution increases from a small value for conventional alloys to a large value for high-entropy alloys of the composition [2].

Based on the effect of entropy of mixing, it is possible to divide the variety of alloys into three fields, as shown in Figure 7b. Low entropy alloys are traditional alloys. High-entropy alloys are alloys with at least five basic elements. Medium entropy alloys are alloys with 2–4 basic elements. The high-entropy effect of activation of the formation of a disordered solid phase occurs in essence in the field of high-entropy alloys and should be present to a lesser extent in medium-entropy alloys. Stabilization of a simple solid solution phase is important for the microstructure and properties that can be obtained in these materials [2].

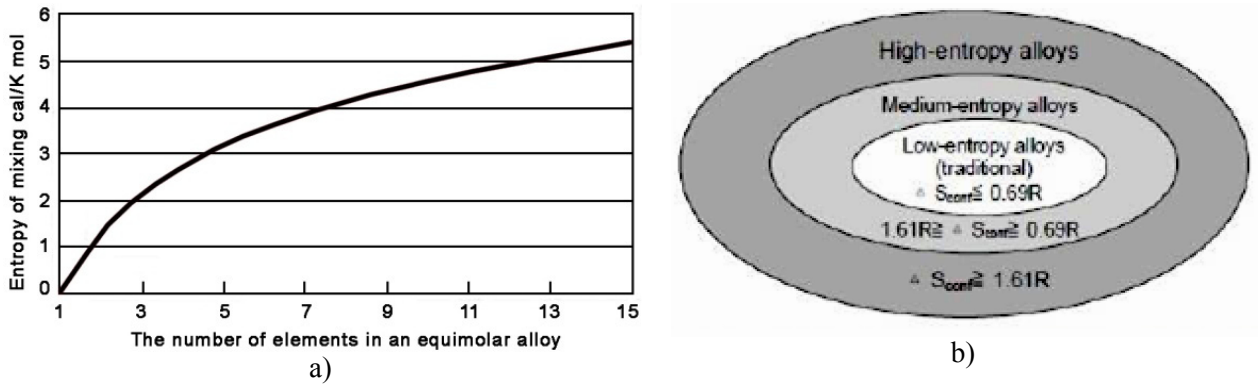

a) b)

Figure 7. The increase in the entropy of mixing to the number of elements in equimolar alloys in a disordered state (a), the division of the world of alloys by the entropy of mixing (b) [2].

It should be noted that the thickness of the surface layer equal to R(I) = M / ρ for high-entropy alloys is significantly lower than for structures of 4-5 and more elemental composition (Table 3) [18]. Table 3 shows that the thickness of the surface layer R(I) of the most common crystals is an order of magnitude greater than the thickness of the surface layer of high-entropy alloys.

Table 3

Thickness of the surface layer of complex crystals [18]

Group of pomegranate	R(I), nm	Group of pomegranate	R(I), nm
$Mg_3Al_2(SiO_4)_3$	25,9	$Ca_3Fe_2Si_3O_{12}$	21,1
$Fe_3Al_2(SiO_4)_3$	19,7	$Ca_3Ti_2(Fe_2Si)O_{12}$	22,7
$Mn_3Al_2[SiO_4]_3$	19,6	$Ca_3Fe_2(SiO_4)_3$	18,8
$Ca_3Al_2[SiO_4]_3$	21,7	$Ca_3(VAlFe)_2(SiO_4)_3$	26,2

This indicates a strong compression of the crystal lattice, reducing its molar (atomic) volume according to equation (5).

Comparing the thickness of the surface layer of high-entropy alloys from Table 2 with the thickness of the surface layer of metallic glasses, we found a great similarity (Table 4), R(I) is not more than 2 nm [28].

In our opinion, there is a lot in common between high-entropy alloys and metallic glasses. Let's compare the mechanical properties of high-entropy alloys, metallic glasses and traditional stainless steels. Table 5 shows that the microhardness of high-entropy alloys and metallic glasses is approximately the same, but 2-3 times higher than that of stainless alloys. This means that the mechanisms for the formation of high-entropy alloys are similar to those for the formation of metallic glasses.

The first metallic glass $Au_{75}Si_{25}$ was obtained by group in the USA in 1960 [29], and the first high-entropy alloy was obtained by Chinese researchers in 2004 [1-3], that is, 40 years later than metallic glasses.

Table 4

Thickness of the surface layer of metallic glass [28]

Glass	M, g/mol	ρ, g/sm^3	R(I), nm
$Mg_{65}Cu_{25}Y_{10}$	40,7	3,8	1,8
$Pd_{40}Ni_{40}P_{20}$	72,3	8,9	1,4
$Fe_{78}Si_{10}B_{12}$	47,6	6,7	1,2
$Ti_{50}Be_{50}Zr_{10}$	36,6	3,7	1,7
$Fe_{40}Ni_{40}P_{14}B_6$	50,8	7,2	1,2
$Ni_{49}Fe_{29}P_{14}B_6Al_2$	56,7	7,8	1,2
$Zr_{62}Cu_{22}Al_{10}Fe_5Dy_1$	77,6	7,0	1,9
$Zr_{41.2}Ti_{13.8}Cu_{12.5}Ni_{10}Be_{22.5}$	53,8	5,7	1,6

Table 5

Microhardness μ of high-entropy alloys (HEA), metallic glasses (MS) and stainless steels (NS)

HEA	μ, HV [10]	MS	μ, HV [30]	NS	μ, HV [21]
FeCrNiTiZrAl (our alloy)	585	$Fe_{80}B_{20}$	1100	316 Stainless steel	189
CoCrFeNiMn	659	$Fe_{78}Mo_2B_{20}$	1015	17-4 PH Stainless steel	410
CrNiTiZrCu	890	$Fe_{40}Ni_{40}P_{14}B_6$	640	Stellite 6 (base Co-Cr)	413
AlTiVFeNiZr	800	$Fe_{78}P_{13}C_7$	760	Hastelloy C (based on Ni-Mo-Fe)	236
MoTiVFeNiZr	740	$Fe_{78}Si_{10}B_{12}$	890	18X2H4MA	269
CuTiVFeNiZrCo	630	$Ni_{75}Si_8B_{17}$	860	15XCHД	335
MoTiVFeNiZrCo	790	$Co_{75}Si_{15}B_{10}$	910	20ХГНР	197

Let us now turn to Table 2 and consider the anisotropy of the surface energy of FeCrNiTiZrAl. Table 2 shows that the maximum surface energy σhkl is achieved in the [111] plane. Metals with a face-centered cubic (fcc) lattice are deformed along close-packed octahedral [111] planes in close-packed <110> directions. In cube-shaped lattices along the direction of the edge there are fewer atomic units than the diagonal of the cube in the bcc lattices or the diagonal of the fcc face, where there are more atomic units. The same is true for the planes that intersect the faces of the bcc and fcc lattices. Since atomic units differ in different crystallographic directions, and hence their density differs, this leads to the fact that the physical and chemical properties exhibit anisotropy of these properties in crystalline solids.

It is rather difficult to experimentally study the energy of the surface of a solid, because the atoms are not in a liquid, where they are mobile, but rather strongly linked by intermolecular interactions. They become mobile only at a temperature close to the melting point of a solid. At room and lower temperatures, the surface energy of a crystal can be determined only by knowing its crystal structure, that is, only in the case when it is possible to do the work of splitting the crystal in one direction or another, if the destruction of the solid itself was brittle [31]. This method was developed in 1930 by Obreimov [32] and consisted of splitting the crystal along the cleavage plane, which bends and the connected dynamometer measures the force preventing this. The work of this force gives the value of surface energy. Gilman [33] (Table 6) measured the surface energy of a number of crystals using this method at the temperature of liquid nitrogen (T = -196ºC). The error obtained in determining the surface energy by the method of splitting a crystal is from 10 to 20%. Comparing tables 6 and 2, we find that magnesium oxide and silicon oxide have similar values of surface energy for HEAs if we take into account that these values were obtained in experiments at T = -196ºC.

Table 6

Surface energy of some crystals [33]

Crystal	LiF (100)	MgO (100)	CaF_2 (111)	$CaCO_3$ (100)	Si (111)	Zn (0001)
σ_s, mJ/m^2	340	1200	450	230	1240	105

The anisotropy of the surface energy leads to the fact that the melting temperature of various faces becomes different and, with a decrease in the particle size, it changes according to the law [34]:

$$T(r) = T_0\left(1 - \frac{R(I)}{r}\right), \tag{9}$$

where T_0 is the melting point of the bulk sample.

Table 7 shows the coefficients of friction FeCrNiTiZrAl, measured by us on the installation in Figure 5b. The average values are ~ 0.06, which noticeably distinguishes them from traditional steels, where the steel-steel friction coefficients are ~ 0.8.

Table 7

Coefficients of friction of samples sprayed for 2 hours in argon

Number of measurements	Coefficients of friction of samples with FeCrNiTiZrAl sputtering	
	over copper plate	over aluminum plate
1	0,075	0,044
2	0,067	0,091
3	0,092	0,044
4	0,076	0,059
5	0,074	0,062
6	0,072	0,047
7	0,086	0,054
8	0,074	0,050
9	0,092	0,055
10	0,109	0,050
Average	**0,081**	**0,055**

Within the framework of the thermodynamic approach for the dry friction coefficient, we obtained the following formula [34]:

$$k = \tilde{N} \cdot \dot{O} \cdot \frac{\sigma \cdot S}{\Delta G^0} \cdot \overline{N}, \quad (10)$$

where σ is the specific surface energy of the material, S is the contact area, T is the temperature, ΔG^0 is the Gibbs energy, $\overline{N}$ is the average number of elementary fracture carriers (proportional to the number of defects), C is a constant.

But according to the molecular kinetic theory, the friction force F ~ k is equal to:

$$F = \int \sigma dL \approx \sigma \cdot L, \quad (11)$$

where σ is the surface energy (table 2), L is the length of the traveled path.

Equation (10) shows that the coefficient of friction is proportional and increases with increasing surface energy according to (11), that is, the value of σ from Table 2 should lead to an increase in the coefficient of friction. But the opposite picture is observed experimentally, the friction coefficient decreases, which contradicts the molecular kinetic theory but becomes explainable from the point of view of our formula (10), which contains the Gibbs formula in the denominators and significantly decreases for a high-entropy alloy according to formulas (8) and (1). Since tribological properties play an essential role in technology, high-entropy alloys and coatings will take a worthy place among structural materials.

Let us now turn to Figure 4, where AFM images show the waviness of the surface. We measured the microhardness multiple times every 0.5 mm on an electronic microhardness tester HVS-1000A. The results are shown in Figure 8.

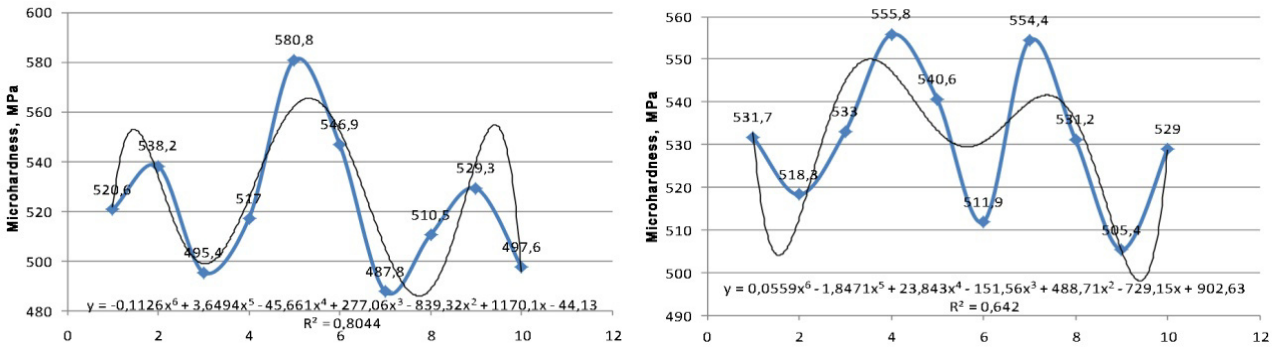

Figure 8. Autowaves in the FeCrNiTiZrAl coating [35]

In both cases, a quasiperiodic structure is observed, i.e., wave process. Figure 8 shows that the wavelength is about 10^{-4} m, i.e., the mass transfer rate is ~ 10^{-4} m/s. Since the rate of mass transfer $V \approx \sqrt{D/t}$, then for the diffusion coefficient we obtain the estimate D ~ 10^{-8} m^2/s. This corresponds to the low diffusion regime [36].

We considered the problem of crystallization of a deposited coating in the form of a cylinder of finite dimensions with a movable interface. The non-stationary equation describing this process in a movable cylindrical coordinate system moving according to the law β(t) has the form [37-39]:

$$\frac{\partial T}{\partial t} = \alpha\left[\frac{\partial^2 T}{\partial z^2} + \frac{1}{r}\frac{\partial}{\partial r}\left(r\frac{\partial T}{\partial r}\right)\right], \qquad (12)$$

where α is the coefficient of thermal diffusivity.

As a result, the solution is obtained in the form:

$$T(r,z) = \frac{T_0 R}{\sqrt{\pi z}} I_0\left(\frac{2r}{R}\right).$$

The radial and axial components of the temperature gradient are equal:

$$\frac{\partial T}{\partial r} = \frac{2}{z}\frac{T_0}{\sqrt{\pi}} I_1\left(\frac{2r}{R}\right),$$

$$\frac{\partial T}{\partial z} = \frac{R T_0}{\sqrt{\pi z^2}} I_0\left(\frac{2r}{R}\right).$$

Both equations containing the Bessel functions $I_0(2r/R)$ and $I_1(2r/R)$ show the wave character of the coating solidification (Fig. 9).

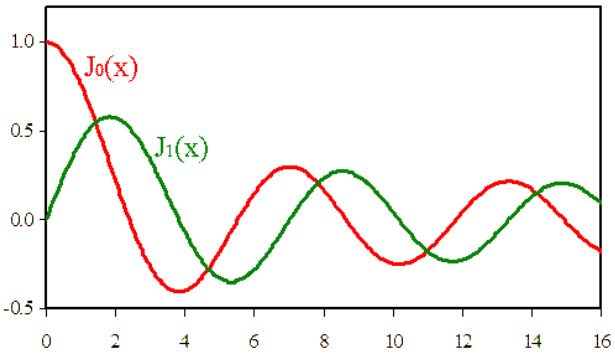

Figure 9. Graphs of Bessel functions (compare with Figure 8)

The theory of crystallization of a cylinder of finite dimensions developed by us belongs to problems with a moving phase interface and is called the Stefan problem [40]. Boundary value problems of this type differ significantly from the classical problems of heat conduction or diffusion. This difference is associated with the motion of the phase separation according to an arbitrary law, so that the separation of variables by classical methods is not feasible. The method of integral Fourier transforms is also not allowed. The motion of the phase boundary leads to nonlinearity of the system of equations, which causes the appearance of autowaves.

Industrial testing of high-entropy coating

At Karaganda CHPP-3, a hammer mill that has high economic indicators is used in systems with direct fuel injection and can work under pressure. In these mills the fuel is crushed mainly by the impact of hammers (beats), and partially also abrades between the beaters and the mill body. The main problem in the operation of coal grinding mills is the high abrasive wear of the beaters, the service life of which averages 500 hours.

In this work, an attempt is made to increase the service life of the beaters of coal grinding mills by mechanically activating them in a tumbling drum, followed by the application of hardening coatings from high-entropy FeCrNiTiZrAl alloys (Fig.10a). Studies have shown that with the FeCrNiTiZrAl coating the microhardness increases by about 1.6 times; wear resistance increases 7.5 times; the coefficient of friction decreas-

es almost 10 times, and the resource of the beater increases almost three times, which is economically very significant.

The turbomechanical plant in Karaganda mastered the blades for the T-100/120-130-2 TMZ steam turbine. It is a single-shaft three-cylinder unit with two cogeneration steam extractions (upper and lower) and two exhausts. The main cause of erosive wear of the blades of low-pressure stages of steam turbines is cavitation phenomena during the shock-droplet effect of wet steam on certain zones of the blades during the operation of the turbine. Coating was carried out on prepared turbine blades made of steel grade 20X13. The vacuum chamber was evacuated to a pressure of 0.003 Pa, then the PINK was switched on, Ar was injected to a pressure of 1 Pa, a negative bias potential of 1000 V was applied to the substrate, and the blade surface was cleaned and heated for 10 min. Then the argon pressure was lowered to 0.1 Pa, and the magnetron was turned on. The displacement on the blades was reduced to 150 V, the magnetron current was kept constant 3 A. The blades were located in the chamber at a distance of 15 cm, the spraying time was 1 hour. Turbine blades with spraying are shown in Figure 10 b.

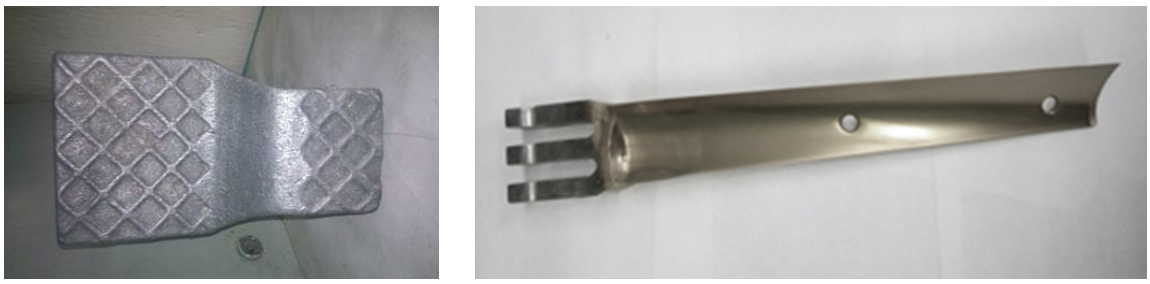

a) b)

Figure 10. Beater for coal grinding mills coated with FeCrNiTiZrAl (a), turbine blades coated with FeCrNiTiZrAl (b).

Conclusion

In our proposed empirical model, the surface anisotropy and the thickness of the surface layer of the high-entropy FeCrNiTiZrAl alloy are calculated. X-ray fluorescence electron spectroscopy of FeCrNiTiZrAl coatings for argon and chemical composition showed that we have formed a high-entropy alloy, the thickness of the surface layer of which was 2 nm. In our opinion, there is a lot in common between high-entropy alloys and metallic glasses. Comparison shows that the microhardness of high-entropy alloys and metallic glasses is approximately the same, but 2-3 times higher than that of stainless alloys. This means that the mechanisms for the formation of high-entropy alloys are similar to those for the formation of metallic glasses.

Studies have shown that the maximum surface energy σhkl is reached in the [111] plane. Metals with a face-centered cubic (fcc) lattice are deformed along close-packed octahedral [111] planes in close-packed <110> directions. The anisotropy of the surface energy leads to the fact that the melting point of different faces becomes different and with a decrease in the size of the coating, it changes according to the hyperbolic law.

The equation (10) we obtained shows that the friction coefficient is proportional and increases with an increase in the surface energy according to (11), that is, the value of σ should lead to an increase in the friction coefficient. But the opposite picture is observed experimentally, the friction coefficient decreases, which contradicts the molecular-kinetic theory but becomes explainable from the point of view of our formula (10), which contains the Gibbs formula in the denominators and decreases significantly for the high-entropy one. Since tribological properties play an essential role in technology, high-entropy alloys and coatings will take a worthy place among structural materials.

The wear of the Hadfield steel used at CHPP-3 occurs in (500-550) hours of continuous operation. That is, after the high-entropy coating of FeCrNiTiZrAl, the resource of the mill increases almost 3 times, which is economically very significant.

The microhardness of our FeCrNiTiZrAl coating is not inferior to high-entropy equiatomic alloys. Such wear resistance of the FeCrNiTiZrCu coating means that the structure of the coating is not only high-entropy, as evidenced by the chemical composition, but also ordered. The ordering of the coating corresponds, as a rule, to dissipative structures. They differ from equilibrium structures in that for their existence they require a constant influx of energy from the outside (magnetron deposition of a coating).

The work was performed under the program of the Ministry of Education and Science of the Republic of Kazakhstan. Grants No. 0118RK000063 and No. F.0781.

References

1 Yeh J.-W. Nanostructured High-Entropy Alloys with Multiple Principle Elements: Novel Alloy Design Concepts and Outcomes / J.-W. Yeh, S.-K. Chen, S.-J. Lin, Sh.-Y. Chang// Advanced Engineering Materials. — 2004. — Vol. 6, №8. — P. 299-303.

2 Yeh J.W. High-entropy alloys — a new era of exploitation / J.W. Yeh, Y.L. Chen, S.J. Lin // Materials Science Forum. — 2007. — Vol. 560. — P. 1-9.

3 Wang Y.P. Solid Solution or Intermetallics in a High-Entropy Alloy / Y.P. Wang, B.Sh. Li, Zh.F. Heng // Advanced Engineering Materials. — 2009. — Vol. 11, № 8. — P. 641-644.

4 Firstov S.A. A new class of materials — high-entropy alloys and coatings / S.A. Firstov, V.F. Gorban, N.A. Krapivka, E.P. Pechkovsky // Vestnik TSU, — 2013. — Vol. 18. — P. 1938-1940.

5 Shaginyan L.R. Properties of coatings from high-entropy alloy Al–Cr–Fe–Co–Ni–Cu–V obtained by magnetron sputtering / L.R. Shaginyan, V.F. Gorban, N.A. Krapivka, S.A. Firstov, I.F. Kopylov // Superhard materials. — 2016. — No. 1. — P. 33-43.

6 Kostyuk G.I. Scientific foundations for the creation of high-entropy nitride, carbide, boride and oxide nanocoatings on T12A hard alloy / G.I. Kostyuk, Yu, A. Sysoev, O.M. Melkozerova // Open information and computer integrated technologies. — 2017. — No. 75. — P. 121-131.

7 Gorban V.F. Obtaining and physical and mechanical properties of high-entropy oxide based on equiatomic alloy CrFeCoNiMn / V.F. Gorban, A.A. Andreev, A.M. Chikryzhov, M.V. Karpets, A.A. Ostroverkh // Superhard materials. — 2019. — No. 1. — P. 51-57.

8 Sanin V.N. SHS metallurgy of cast high-entropy alloys based on transition metals / V.N. Sanin, V.I. Yukhvid, D.N. Ikornikov // *DAN NAN*. — 2016. — Vol. 470. — No. 4. — P. 421-426.

9 Miracle D.B. A critical review of high entropy alloys and related concepts / D.B. Miracle, O.N. Senkov // Acta Mater. — 2017. — Vol. 122. — P. 448–511.

10 Шайсултанов Д.Г. Структура и механические свойства высокоэнтропийных сплавов системы CoCrFeNiX (X = Mn, V, Mn и V, Al и Cu): дис. ... канд. техн. наук // Д.Г. Шайсултанов. — Белгород, 2015. — 142 с.

11 Ивченко М.В. Структура, фазовые превращения и свойства высокоэнтропийных эквиатомных металлических сплавов на основе AlCrFeCoNiCu: дис. ... канд. физ.-мат. наук // М.В. Ивченко. — Екатеринбург, 2015. — 167 с.

12 Юрченко Н.Ю. Разработка и исследование высокоэнтропийных сплавов с высокой удельной прочностью на основе системы Al-Cr-Nb-Ti-V-Zr: дис. ... канд. тех. наук // Н.Ю. Юрченко. — Белгород, 2019. — 187 с.

13 Yurov V.M. Wear resistance and tribological properties of high entropy coatings CrNiTiZrCu / V.M. Yurov, E.N. Eremin, S.A. Guchenko // Eurasian Physical Technical Journal. — 2020. — Vol. 17. — No. 1 (33). — P. 13–18.

14 Yurov V.M. Structural properties of the high-entropy TiNiZrCuCr coating / V.M. Yurov, S.A. Guchenko, K.M. Makhanov // Modern science-intensive technol. — 2020. — No. 4. — P. 78-83.

15 Yurov V.M. Application of high-entropy coatings on turbine blades / V.M. Yurov, B.N. Shelpyakov, S.A. Guchenko, A.N. Tvardovsky // Trends in the development of science and education. — 2020. No. 59, Part 1. — P. 49-54.

16 Yurov V.M. Anisotropy of surface energy and thickness of the surface layer of magnetic nanostructures / V.M. Yurov, V.I. Goncharenko, V.S. Oleshko // Nano- and microsystem technology. — 2021. — V. 23, No. 2. — P. 59-62.

17 Yurov V.M. Anisotropy of the surface energy of silicon. Bulletin of KazNU im. al Farabi // V.M. Yurov. — 2021. — No. 1(76). — P. 51-58.

18 Yurov V.M. Surface layer thickness, surface energy, and atomic volume of an element / V.M. Yurov, S.A. Guchenko, V.Ch. Laurinas // Physicochemical aspects of the study of clusters, nanostructures and nanomaterials. — 2018. Issue. 10. — P. 691-699.

19 Bokarev V.P. Anisotropy of physicochemical properties of single-crystal surfaces / V.P. Bokarev, G.Ya. Krasnikov // Electronic engineering. Series 3. Microelectronics. — 2016. — No. 4 (164). — P. 25-30.

20 Бочкарев В.П. Развитие физико-химических принципов оценки влияния поверхностной энергии на свойства материалов и процессы для технологии микроэлектроники: дис. ... д-ра техн. наук // В.П. Бочкарев. — М., 2020. — 299 с.

21 Солнцев Ю.П. Металлы. Справочник / Ю.П. Солнцев. — СПб.: Рубин, 2000. — 614 с.

22 Arutyunov K.Yu. Quantum size effects in metallic nanostructures / K.Yu. Arutyunov // DAN VSH RAS. — 2015. — No. 3(28). — P. 7-16.

23 Оура К. Введение в физику поверхности / К. Оура, В.Г. Лифшиц, А.А. Саранин, А.В. Зотов, М. Катаяма. — М.: Наука, 2006. — 490 с.

24 Uvarov N.F. Size effects in the chemistry of heterogeneous systems / N.F. Uvarov, V.V. Boldyrev // Uspekhi khimii. — 2001. — V. 70 (4). — P. 307-329.

25 Gusev A.I. Nanomaterials, nanostructures, nanotechnology / A.I. Gusev. — Moscow: Fizmatlit, 2005. — p. 96.

26 Андриевский Р.А. Наноструктурные материалы / Р.А. Андриевский, А.В. Рагуля. — М.: Академия, 2005. — 192 с.

27 Суздалев И.П. Нанотехнология: физико-химия нанокластеров, наноструктур и наноматериалов / И.П. Суздалев. — М.: КомКнига, 2006. — 592 с.

28 Yurov V.M. Surface and surface energy of metal glasses / V.M. Yurov, D.A. Kaykenov // Sciences of Europe. — 2020. — No. 51. — Vol. 1. — P. 71-74.

29 Cheng Y.Q. Atomic-level structure and structure–property relationship in metallic glasses / Y.Q. Cheng, E. Ma // Progress in Materials Science. — 2011. — Vol. 56. — P. 379 — 473.

30 Абросимова Г.Е. Эволюция структуры металлических стекол при внешних воздействиях: дис. д-ра физ.-мат. наук // Г.Е. Абросимова. — Черноголовка, 2012. — 296 с.

31 Kudrya A.V. The role of different-scale structures in ensuring the plasticity and toughness of structurally inhomogeneous steels / A.V. Kudrya // Metallurgy and heat treatment of metals. — 2005. — No. 5. — P. 18-23.

32 Obreimoff, J.W. The splitting reigth of mica / J.W. Obreimoff // Proc. Roy. — 1930. — V. 127. — P. 290-293.

33 Gilman J. Direct Measurements of the surface energies of crystals / J. Gilman // J. Appl. Phys., — 1960. — Vol. 31, № 2. — P. 2208-2216.

34 Yurov V.M. Estimation of the melting temperature of nanostructures of solids / V.M. Yurov, K.M. Makhanov // Nano- and microsystem technology. — 2020. — Vol. 22, No. 7. — P. 347-351.

35 Yurov V.M. Superfecial tension of pure metals / V.M. Yurov // Eurasian Physical Technical journal. — 2011. — Vol. 8, № 1(15). — P. 10-14.

36 Мищенко Е.Ф. Автоволновые процессы в нелинейных средах с диффузией / Е.Ф. Мищенко, В.А. Садовничий, А.Ю. Колесов, Н.Х. Розов. — М.: Физматлит, 2010. — 395 с.

37 Yurov V.M. Thermodynamics of luminescent systems / V.M. Yurov // Bulletin of the university of Karaganda-Physics. — 2005. — № 3 (39). — P. 13-15.

38 Yurov V.M. The thickness of the surface layer and autowave processes in high-entropy coatings / V.M. Yurov, S.V. Guchenko, K.M. Makhanov // Matrix of scientific knowledge. — 2020. — №. 7. — P. 9-16.

39 Yurov V.M. Application of high entropy coatings simultaneous in one cycle spraying three cathodes / V.M. Yurov, E.N. Eremin, S.A. Guchenko // Bulletin of the university of Karaganda-Physics. — 2020. — № 1 (97). — P. 7-17.

40 Gupta S.C. The Classical Stefan Problem: Basic Concepts, Modelling and Analysis with Quasi-Analytical Solutions and Methods / S.C. Gupta // New Edition: Elsevier. — 2018. — 732 p.

В.М. Юров, А.Т. Бердібеков, Н.А. Белгібеков, Қ.М. Маханов

Жоғарыэнтропиялы FeCrNiTiZrAl жабындары және олардың қасиеттері

Авторлар ұсынған эмпирикалық модельде жоғарыэнтропиялы FeCrNiTiZrAl қорытпасының беткі энергия анизотропиясы және беткі қабаттың қалыңдығы есептелген. Қорытпаның беткі қабатының қалыңдығы шамамен 2 нм құрайды, бұл күрделі кристалдардың беткі қабатының қалыңдығынан үлкен болса да, дегенмен, реті бойынша металл шыныларымен сәйкес келеді. Жоғарыэнтропиялы қорытпаның қаттылығы және басқа да қасиеттері металл шынылардікімен бірдей, бірақ тотығуға төзімді болаттардың қаттылығынан 2-3 есе жоғары. Жоғарыэнтропиялы FeCrNiTiZrAl қорытпасының беттік энергиясы шамамен 2 Дж/м^2 құрайды, бұл магний оксиді мен балқу температурасы жоғары басқа кристалдардың беткі энергиясына сәйкес келеді. Бірақ бұл кристалдардан айырмашылығы, жоғарыэнтропиялы қорытпаның үйкеліс коэффициенттері қарапайым болаттарға қарағанда (~ 0,8) әлдеқайда төмен (~ 0,06). Үйкеліс коэффициенті беткі энергияға пропорционал түрде тәуелді екенін және жоғарыэнтропиялы қорытпа үшін едәуір азайып төменгі үйкеліске әкелетін Гиббс энергиясынан тәуелділігі кері пропорционал екенін теориялық тұрғыдан көрсетілген, жоғарыэнтропиялы қорытпаның жоғары қаттылығымен үйкеліс коэффициентінің төмендігі оларды металдан жасалған конструкциялық бұйымдардың бетіне қалыптастыруға ықпал етіп, осы бұйымдардың қолданысын кеңейтуге оң әсерін тигізеді.

Кілт сөздер: жоғарыэнтропиялық жабындар, қаттылық, үйкеліс, тозуға төзімділік, нанокұрылым, микроқаттылық.

В.М. Юров, А.Т. Бердибеков, Н.А. Бельгибеков, К.М. Маханов

Высокоэнтропийные покрытия FeCrNiTiZrAl и их свойства

В предложенной авторами эмпирической модели рассчитаны анизотропия поверхностной энергии и толщина поверхностного слоя высокоэнтропийного сплава FeCrNiTiZrAl. Толщина слоя поверхности этого сплава составляет около 2 нм, которая на порядок превышает толщину поверхностного слоя сложных кристаллов, но имеет такой же порядок, как и металлические стекла. Твердость и другие свойства высокоэнтропийного сплава одинаковы с металлическими стеклами, но в 2–3 раза превышают твердость нержавеющих сталей. Поверхностная энергия высокоэнтропийного сплава FeCrNiTiZrAl составляет около 2 Дж/м^2, что соответствует поверхностной энергии окиси магния и другим кристаллам с высокой температурой плавления. Но, в отличие от этих кристаллов, коэффициенты трения у высокоэнтропийного сплава значительно ниже (~ 0,06), чем у обычных сталей (~ 0,8). Теоретически нами показано, что коэффициент трения пропорционально зависит от поверхностной энергии и обратно пропорционально зависит от энергии Гиббса, которая значительно уменьшается для высокоэн-

тропийного сплава, приводя к низкому трению. Высокая твердость и низкий коэффициент трения высокоэнтропийного сплава способствуют нанесению покрытий из них на конструкционные изделия из металлов, что способствует их широкому применению.

Ключевые слова: высокоэнтропийные покрытия, твердость, трение, износостойкость, наноструктура, микротвердость.

References

1 Yeh, J. -W., Chen, S. -K., Lin, S. -J., & Chang, Sh. -Y. (2004). Nanostructured High-Entropy Alloys with Multiple Principle Elements: Novel Alloy Design Concepts and Outcomes. *Advanced Engineering Materials*, 6, № 8, 299-303.

2 Yeh, J.W., Chen, Y.L., Lin, S.J. (2007). High-entropy alloys — a new era of exploitation. *Materials Science Forum*, 560, 1-9.

3 Wang, Y.P., Li, B.Sh., Heng, Zh.F. (2009). Solid Solution or Intermetallics in a High-Entropy Alloy. *Advanced Engineering Materials*, 11, № 8, 641-644.

4 Firstov, S.A., Gorban, V.F., Krapivka, N.A., & Pechkovsky E.P. (2013). A new class of materials — high-entropy alloys and coatings. *Vestnik TSU*, 18, 1938-1940.

5 Shaginyan, L.R., Gorban, V.F., Krapivka, N.A., Firstov, S.A. ,& Kopylov, I.F. (2016). Properties of coatings from high-entropy alloy Al–Cr–Fe–Co–Ni–Cu–V obtained by magnetron sputtering. *Superhard materials*, 1, 33-43.

6 Kostyuk, G.I., Sysoev, Yu, A., Melkozerova O.M. (2017). Scientific foundations for the creation of high-entropy nitride, carbide, boride and oxide nanocoatings on T12A hard alloy. *Open information and computer integrated technologies*, 75, 121-131.

7 Gorban, V.F., Andreev, A.A., Chikryzhov, A.M., Karpets, M.V. & Ostroverkh A.A. (2019). Obtaining and physical and mechanical properties of high-entropy oxide based on equiatomic alloy CrFeCoNiMn. *Superhard materials*, 1, 51-57.

8 Sanin, V.N., Yukhvid, V.I., Ikornikov, D.N. (2016). SHS metallurgy of cast high-entropy alloys based on transition metals. *DAN NAN*, 470, 4, 421-426.

9 Miracle, D.B., Senkov, O.N. (2017). A critical review of high entropy alloys and related concepts. *Acta Mater.*, 122, 448–511.

10 Shaisultanov, D.G. (2015). Struktura i mekhanicheskie svoistva vysokoentropiinykh splavov sistemy CoCrFeNiX (X = Mn, V, Mn i V, Al i Cu) [Structure and mechanical properties of high-entropy alloys of the CoCrFeNiX system (X = Mn, V, Mn and V, Al and Cu)]. *Candidate's thesis*. Belgorod [in Russian].

11 Ivchenko, M.V. (2015). Struktura, fazovye prevrashcheniia i svoistva vysokoentropiinykh ekviatomnykh metallicheskikh splavov na osnove AlCrFeCoNiCu [Structure, phase transformations and properties of high-entropy equiatomic metal alloys based on AlCrFeCoNiCu]. *Candidate's thesis*. Yekaterinburg [in Russian].

12 Yurchenko, N.Yu. (2019). Razrabotka i issledovanie vysokoentropiinykh splavov s vysokoi udelnoi prochnostiu na osnove sistemy Al-Cr-Nb-Ti-V-Zr [Development and research of high-entropy alloys with high specific strength based on the Al-Cr-Nb-Ti-V-Zr system]. *Candidate's thesis*. Belgorod [in Russian].

13 Yurov, V.M., Eremin, E.N., Guchenko, S.A. (2020). Wear resistance and tribological properties of high entropy coatings CrNiTiZrCu. *Eurasian Physical Technical Journal*, 17, 1 (33), 13-18.

14 Yurov, V.M., Guchenko, S.A., Makhanov, K.M. (2020). Structural properties of the high-entropy TiNiZrCuCr coating. *Modern science-intensive technol*, 4, 78-83.

15 Yurov, V.M., Shelpyakov, B.N., Guchenko, S.A.,& Tvardovsky, A.N. (2020). Application of high-entropy coatings on turbine blades. *Trends in the development of science and education*, 59, 1, 49-54.

16 Yurov, V.M., Goncharenko, V.I., Oleshko, V.S. (2021). Anisotropy of surface energy and thickness of the surface layer of magnetic nanostructures. *Nano- and microsystem technology*, 23, 2, 59-62.

17 Yurov, V.M. (2021). Anisotropy of the surface energy of silicon. *Bulletin of KazNU im. al Farab*i, 1(76), 51-58.

18 Yurov, V.M., Guchenko, S.A., Laurinas, V.Ch. (2018). Surface layer thickness, surface energy, and atomic volume of an element. *Physicochemical aspects of the study of clusters, nanostructures and nanomaterials,* Issue. 10, 691-699.

19 Bokarev, V.P., Krasnikov, G.Ya. (2016). Anisotropy of physicochemical properties of single-crystal surfaces. *Electronic engineering. Series 3. Microelectronics*, 4 (164), 25-30.

20 Bochkarev, V.P. (2020). Razvitie fiziko-khimicheskikh printsipov otsenki vliianiia poverkhnostnoi energii na svoistva materialov i protsessy dlia tekhnologii mikroelektroniki [Development of physicochemical principles for assessing the effect of surface energy on the properties of materials and processes for microelectronic technology]. *Doctor's thesis*. Moscow [in Russian].

21 Solntsev, Yu.P. (2000). *Metally: Spravochnik [Metals. Directory]*. Saint Petersburg: Rubin [in Russian].

22 Arutyunov, K.Yu. (2015). Quantum size effects in metallic nanostructures. *DAN VSH RAS*, 3(28), 7-16.

23 Oura, K., Lifshits, V.G., Saranin, A.A., Zotov, A.V., & Kataiama, M. (2006). *Vvedenie v fiziku poverkhnosti [Introduction to surface physics]*. Moscow: Nauka [in Russian].

24 Uvarov, N.F., Boldyrev, V.V. (2001). Size effects in the chemistry of heterogeneous systems. *Uspekhi khimii*, 70 (4), 307-329.

25 Gusev, A.I. (2005). *Nanomaterials, nanostructures, nanotechnology*. Moscow: Fizmatlit.

26 Andrievskii, R.A., & Ragulia, A.V. (2005). *Nanostrukturnye materialy [Nanostructured materials]*. Moscow: Akademiia [in Russian].

27 Suzdalev, I.P. (2006). *Nanotekhnologiia: fiziko-khimiia nanoklasterov, nanostruktur i nanomaterialov [Nanotechnology: physical chemistry of nanoclusters, nanostructures and nanomaterials]*. Moscow: KomKniga [in Russian].

28 Yurov, V.M., Kaykenov, D.A. (2020). Surface and surface energy of metal glasses. *Sciences of Europe*, 51, 1, 71-74.

29 Cheng, Y.Q., Ma, E. (2011). Atomic-level structure and structure–property relationship in metallic glasses. *Progress in Materials Science*, 56, 379–473.

30 Abrosimova, G.E. (2012). Evoliutsiia struktury metallicheskikh stekol pri vneshnikh vozdeistviiakh [Evolution of the structure of metallic glasses under external influences] *Doctor's thesis*. Chernogolovka [in Russian].

31 Kudrya, A.V. (2005). The role of different-scale structures in ensuring the plasticity and toughness of structurally inhomogeneous steels. *Metallurgy and heat treatment of metals*, 5, 18-23.

32 Obreimoff, J.W. (1930). The splitting reigth of mica. *Proc. Roy,* 127, 290-293.

33 Gilman, J. (1960). Direct Measurements of the surface energies of crystals. *J. Appl. Phys.*, 31, № 2, 2208-2216.

34 Yurov, V.M., Makhanov, K.M. (2020). Estimation of the melting temperature of nanostructures of solids. *Nano- and microsystem technology*, 22, 7, 347-351.

35 Yurov, V.M. (2011). Superfecial tension of pure metals. *Eurasian Physical Technical journal*, 8, № 1 (15), 10-14.

36 Mishchenko, E.F., Sadovnichii, V.A., Kolesov, A.Yu., & Rozov, N.Kh. (2010). *Avtovolnovye protsessy v nelineinykh sredakh s diffuziei [Autowave processes in nonlinear media with diffusion]*. Moscow: Fizmatlit [in Russian].

37 Yurov, V.M. (2005). Thermodynamics of luminescent systems // *Bulletin of the university of Karaganda-Physics*, 3 (39), 13-15.

38 Yurov, V.M., Guchenko, K.M., Makhanov, K.M. (2020). The thickness of the surface layer and autowave processes in high-entropy coatings. Matrix of scientific knowledge. 7, 9-16.

39 Yurov ,V.M., Eremin, E.N., & Guchenko, S.A. (2020). Application of high entropy coatings simultaneous in one cycle spraying three cathodes. *Bulletin of the university of Karaganda-Physics*, 1 (97), 7-17.

40 Gupta, S.C. (2018). The Classical Stefan Problem: Basic Concepts, Modelling and Analysis with Quasi-Analytical Solutions and Methods. New Edition: Elsevier.